X-621-66-573

NASA TM X- 55760

ON THE ION COMPOSITION AND TEMPERATURE IN THE TOPSIDE IONOSPHERE

DECEMBER 1966

GODDARD SPACE FLIGHT CENTER

GREENBELT, MARYLAND

X-621-66-573

ON THE ION COMPOSITION AND TEMPERATURE IN THE TOPSIDE IONOSPHERE

H. G. Mayr, L. H. Brace, and G. S. Dunham
Aeronomy Branch

December 1966

GODDARD SPACE FLIGHT CENTER
Greenbelt, Maryland

ON THE ION COMPOSITION AND TEMPERATURE IN THE TOPSIDE IONOSPHERE

H. G. Mayr,* L. H. Brace, and G. S. Dunham

Aeronomy Branch

Goddard Space Flight Center

Greenbelt, Maryland

ABSTRACT

In the topside ionosphere, where electrons, ions, and neutrals are not in thermal equilibrium and where $[H^+] \ll [O^+]$, the altitudinal distribution of protons in diffusive equilibrium deviates strongly from that in chemical equilibrium through charge-exchange with O^+. The particle continuity equations for H^+ and O^+ and the energy continuity equation are solved simultaneously by means of a computer program. The processes included are photoionization, charge-exchange, ambipolar diffusion along magnetic field lines, heat conduction, local and nonlocal heating, and heat loss from ions to neutrals. The ion composition and plasma temperature along various field lines are derived and studied by adopting electron density and temperature from Explorer XXII measurements (1000-km altitude, vernal equinox) as boundary conditions. The $O^+ - H^+$ composition transition region at middle and low latitudes is fully described. It is found that a neutral hydrogen concentration of $2 \times 10^5/cc$ at 500 km is required to make the calculated electron density consistent with satellite measurements of electron density at 650 km. A latitudinal variation of the ion composition arises primarily because of the latitudinal variation of the electron temperature. The ion transition level at 800 km around the equator increases to 1000 km near 40° latitude during midday. During nighttime, the transition level decreases to approximately 600 km because of the decrease of electron temperature and neutral oxygen concentration. Solving the energy equation for the plasma temperature shows that the temperature gradient along field lines is a function of latitude. The temperature decreases for example along the equatorial field line that passes through the equator at 1000 km and increases along the 40° field line. This causes the equatorial trough of the electron temperature shown from Explorer XXII and also explains the latitudinal variation of the calculated ion composition, which in turn agrees with OGO-C and other ion composition measurements.

*NAS-NRC resident research associate

ON THE ION COMPOSITION AND TEMPERATURE IN THE TOPSIDE IONOSPHERE

INTRODUCTION

From satellite experiments (H. Taylor et al, 1966) in the topside ionosphere, evidence arises for the latitudinal variation of the ion composition. At a constant altitude, the proportion of oxygen ions is greater at higher latitudes and, accordingly, that of hydrogen ions is less. This tendency is less pronounced at night. The main purpose of this paper is to study theoretically this behavior of the ion species; which, in view of the different ion masses and correspondingly different scale heights, is also of interest in understanding the electron density variation in the topside ionosphere.

Brace and Reddy (1965) and Brace, Reddy, and Mayr (1967) derived latitudinal electron density and temperature profiles from the electrostatic probe experiment on Explorer XXII. The results show that the density is relatively high at the equator, and falls off toward increasing latitudes in the daytime. At night, an electron density trough develops at the equator, and enhancements form at middle latitudes. The temperature measurements show a shallow minimum at the equator in the daytime and a broad, trough during nighttime.

Figures 1 and 2 show the Explorer XXII observations of T_e and N_e (Brace, Reddy, Mayr, 1967). Close to the equator, where the Explorer XXII orbit is parallel to the geomagnetic field, spatial derivatives from the latitudinal variation of T_e and N_e were assumed equal to those along the field line. Employing these derivatives and the available time gradients in the motion and energy equations for field-aligned particle and energy transports Brace, Reddy and Mayr came to the following conclusions for the equatorial region at 1000 km.

1. In order to understand the latitudinal and local time variations of the electron temperature and density near the equator at 1000 km, the local energy loss from protons to hydrogen atoms had to be considered as a major cooling process. A neutral hydrogen concentration in the order of 10^5/cc was required to produce the observed temperature trough. This concentration exceeds considerably that given in the Harris and Priester (1964) model. The energy input was assumed to be the result of an escape flux of fast electrons of the order of $10^8/cm^2/sec$, and protons were assumed to be the predominating ion species.

2. The concept of diffusive equilibrium was proved valid, even for the dynamic periods after sunrise and sunset. On this basis, latitudinal variations of temperature and density were found to be mutually self-consistent at the equator. It was shown that the temperature minimum there during daytime contributes to the latitudinal density maximum

observed at the equator, implying a negative temperature gradient along the corresponding field line.

These immediate deductions from Explorer XXII data are valid to the degree that latitudinal variations around the equator actually represent variations along field lines. Secondly, these deductions are restricted to the equatorial region at 1000 km, and they depend on the assumption of a single-ion species (protons) at the equator. The desire to escape from these restrictions led to the investigation described here.

We shall derive in this paper the spatial distributions of electron density and temperature, and of oxygen and hydrogen ions by solving the particle and energy continuity equations. In the following section, we describe these equations and the conditions under which they were solved.

THEORETICAL DISCUSSION

Energy Balance

Through an analysis of Explorer XVII data Brace, Spencer and Dalgarno, (1965) showed that above approximately 500 km, ions and electrons are in thermal equilibrium. We adopted this result as an assumption for our study since it leads to drastic simplifications in the energy and diffusion equations. We realize, however, that the applicability of this assumption depends not only on

altitude but also on latitude, local time, and solar activity. We will discuss this question more thoroughly in a later paper.

For the energy input into the electron-ion gas, we apply a very simple description of the heat sources. Following Geisler and Bowhill (1965) we assume that above 300 km, the local heating rate decreases with the scale height of the neutral oxygen concentration. Thus the heating rate is given by $q[O]$, where q is a constant. The nonlocal heating, which becomes significant above 300 km (Geisler and Bowhill, 1965), we assume is due to a flux of fast electrons, F. These electrons, with energy W, travel along field lines and impart some of their energy to the ambient electrons by means of coulomb collisions.

Following Dalgarno et al, (1963), the rate of heating per fast electron is assumed to be

$$\frac{\partial W}{\partial s} = \frac{K N_e}{W \cos I} ,$$

where

s = distance on a field line,

K = $1.95 \times 10^{-12} eV^2\ cm^2$

N_e = electron density,

I = pitch angle.

For a first approximation we assume that F is constant in view of the large range of fast electrons ($\sim 10^4$ km). This leads to the energy input in the form

$$\frac{2FKN_e}{W\cos I} = pN_e,$$

where the factor 2 is due to fluxes from both the northern and southern hemisphere. Furthermore, we assume, that W and I, and thus p are constant.

The two energy terms, $q[O]$, pN_e, represent the energy input into the electron-ion gas as direct and indirect consequences of the solar UV radiation. They contain uncertainties with respect to the heating efficiency and the fast electron flux, so we considered the constants q and p as parameters to be determined.

For the heat transport within the electron-ion gas we applied the heat conduction of the electrons along the magnetic field which, according to L. Spitzer (1956), is much more effective than that of the ions.

As a cooling mechanism, the energy loss via elastic collisions from ions to neutrals was taken into account. From Brace, Spencer and Dalgarno, 1965, the energy loss is given by

$$K_{x+y}[X^+][Y](T_i - T_n),$$

where

K_{x+y} = coefficient for the local energy loss between ions and neutrals,

$[Y]$ = density of the neutral component Y which is in diffusive equilibrium,

$[X^+]$ = density of the ion component X^+,

T_i = ion temperature,

T_n = neutral temperature.

It turns out that the rate coefficient K_{x+y} for this energy transfer depends very strongly on the ion and neutral species involved in it. For example, the energy loss from hydrogen ions to hydrogen atoms is most effective and exceeds by two orders of magnitude that from oxygen ions to hydrogen atoms and by a factor of 4.4 that from oxygen ions to oxygen atoms.

The light constituents become predominant in both the neutral and charged components of the atmosphere above approximately 500 kilometers. Therefore, in spite of the decrease of the neutral density with altitude, the local cooling of the plasma remains comparable to the fast electron heating up to relatively high altitudes. The difference between heating and cooling produces an appropriate electron temperature gradient through thermal conduction. Thus, knowledge of the ion composition is required in employing the energy equation to calculate the temperature profile. Conversely however, the study of Explorer XXII data (Brace, Reddy, and Mayr, 1966) suggested that the temperature variation effectively controls the ion distribution. Because of this interaction of thermal and

compositional factors, a "chicken or egg" question arises. We avoid this question by solving the energy and particle continuity equations simultaneously.

Particle Balance

Ion composition measurements show, that in the region above 500 km, oxygen and hydrogen ions are the dominating ion constituents for minimum solar activity (Taylor, et al, 1966). Thus we must consider resonance charge transfer from oxygen ions to hydrogen atoms and from hydrogen ions to oxygen atoms as the primary source and sink of protons (after Johnson, 1960). Within the region where H^+ is a minor constituent compared with O^+, the altitude distribution of H^+ for chemical equilibrium coincides with that for diffusive equilibrium (S. Bauer, 1965) when $T_e = T_i = T_n$. This coincidence results in the following simplification of the continuity equation. For a stationary condition, the continuity equation of the hydrogen ions is given in the form

$$- \operatorname{div} j_{H^+} + \frac{9}{8} R [O^+] [H] - R [H^+] [O] = 0, \qquad (1)$$

where

j = transport flux,

R = rate coefficient for charge exchange between hydrogen and oxygen ions ($4.5 \times 10^{-12} T_i^{1/2}$ cm^3 sec^{-1}).

Equation 1 takes into consideration the transport and charge exchange processes.

We can distinguish three different regions in order of increasing altitude. In the lowest region, the charge exchange process predominates, and the proton concentration can be derived from

$$\frac{9}{8} R [O^+] [H] - R [H^+] [O] = 0. \quad (2)$$

Then follows a region in which both transport and chemical processes are of comparable importance. Therefore, the hydrogen ion density is determined by the complete Equation 1. Finally, the highest region is one of fast diffusion where the proton distribution can be derived from

$$\text{div } j_{H^+} = 0 \quad (3)$$

If, as cited before, Equations 2 and 3 lead (for the same boundary condition) to the same proton distribution, then a solution of either Equation 2 or Equation 3 satisfies Equation 1, as long as the condition

$$[H^+] \ll [O^+] \quad (4)$$

is valid. It was shown by Hanson and Ortenburger (1961), that the region of fast diffusion starts where oxygen ions are still the major constituent. If thermal equilibrium ($T_e = T_i = T_n$) existed, the coincidental agreement between the H^+ slopes for diffusive and chemical equilibrium would allow us to apply the equation for diffusive equilibrium throughout the topside ionosphere. However, this

very simple behavior does not occur in the ionosphere where electron, ion, and neutral temperatures are different. In this case the proton distribution for chemical equilibrium differs from that for diffusive equilibrium.

We assume that electrons and ions are in thermal equilibrium at a temperature T_e which does not vary with altitude and is different from the neutral gas temperature T_n. The neutrals are assumed to be in diffusive equilibrium, and we assume that (4) is fulfilled. Following S. Bauer (1965), the altitudinal variation of H^+ in diffusive equilibrium becomes

$$[H^+] = [H^+]_o \exp\left(\frac{z - z_o}{\frac{k T_e}{7 m_p g}}\right), \qquad (5)$$

where

z = altitude,

k = Boltzmann's constant,

T_e = electron temperature,

m_p = proton mass,

g = acceleration of gravity.

Employing the equation of chemical equilibrium (2) leads to a proton distribution

$$[H^+] = \frac{9}{8}\frac{[H][O^+]}{[O]} =$$

$$= \frac{9}{8}\frac{[H]_o[O^+]_o}{[O]_o} \exp\left(\frac{\frac{(z-z_o)}{kT_eT_n}(15T_e - 8T_n)}{m_p g}\right) \cdot \cdot \qquad (6)$$

Transforming Equation 6 into a form similar to Equation 5, gives

$$[H^+] = [H^+]_o \exp\left(\frac{\frac{(z-z_o)}{kT_e^*}}{7m_p g}\right), \qquad (6a)$$

with

$$T_e^* = \frac{7T_eT_n}{(15T_e - 8T_n)}. \qquad (7)$$

For chemical equilibrium the reduced temperature T_e^* corresponds to T_e in diffusive equilibrium. The correlation of Equation 7 is shown in Figure 3. With increasing difference between T_e and T_n, the difference between T_e and T_e^* increases. For example, with T_e = 2000°K. and T_n = 1000°K., T_e^* = 636°K. Thus, for this quite typical condition, the scale height of the hydrogen ions in diffusive equilibrium is larger by approximately a factor of 3 than that for chemical equilibrium. From this we conclude that the lack of complete equilibrium between electron, ion, and gas temperature is an important factor

in describing the behavior of the topside ionosphere. The consequence of this primarily concerns the region described by Equation 1, where it is obvious that the concept of diffusive equilibrium must be dropped. Here chemical and transport processes become coupled, and the entire continuity equation (1) must be solved.

An effect of the charge-exchange reaction becomes evident in the electron density variation with local time at 1000 km (Figure 2). At magnetic latitudes close to ±40°, the electron density increases significantly from daytime to nighttime. In the charge exchange region, described by Equation 6, during nighttime the oxygen density decreases much faster than the O^+ and H^+ concentrations. This causes the proton density to increase and this contributes to the midlatitude enhancement of N_e. Another factor associated with the nighttime N_e enhancement at midlatitude is the electron temperature decrease which causes a downward redistribution of the ions in the protonosphere. The question then arises as to what degree charge-exchange reactions and the temperature variation contribute to this observed midlatitude enhancement. This is another reason to calculate simultaneously the energy and the continuity equations, including the charge-exchange process. In addition we include in the continuity equation the photoionization rates P_O and P_H for neutral oxygen and hydrogen.

Boundary Conditions

The ion continuity equations, as well as the energy equation, are second-order differential equations. For the one-dimensional approach (transport and conduction occurring along field lines), we need two boundary conditions for each equation. One of the boundary conditions is given directly if we postulate that our solutions be symmetrical with respect to the equatorial plane (an approximation of the equinox condition). In this case, all first derivatives of scalar quantities and all vector components along the field line are zero at the equator. For the second boundary condition, the electron temperature must be known, as well as the hydrogen and oxygen ion densities at some level.

In the region of near chemical equilibrium for hydrogen ions, the diffusion term (div j_{H^+}) in the continuity equation is small. Consequently, a definite correlation exists in this region between the oxygen and hydrogen ion concentrations as can be seen from the continuity equation written in the form,

$$[H^+] = \frac{1}{R[O]} \left(- \text{div } j_{H^+} + P_H + \frac{9}{8} R \, [O^+] \, [H] \right) . \qquad (8)$$

Thus O^+ and H^+ are not independent, and therefore we require only a single boundary condition. For this we chose the electron density at some point on the field line. The values of T_e and N_e employed here are those measured from Explorer XXII at 1000 km at equinox (Figures 1 and 2).

Review of the Approach

The basis of our calculation can be summarized as follows:

1. The physical processes entering the ion continuity equations are:
   a. Charge exchange between $[O^+]$ and $[H^+]$,
   b. Photoionization of $[O]$ and $[H]$,
   c. Ambipolar diffusion along geomagnetic field lines.

2. The physical processes involved in the energy equation are the following:
   a. Heat conduction of electrons along field lines,
   b. Local heating due to photoionization,
   c. Nonlocal heating due to fast electrons escaping the F-region,
   d. Local loss from ions to neutrals.

3. T_e is assumed equal to T_i at altitudes considered here (>500 km).

4. The continuity equations for the ion densities are solved simultaneously with the energy equation. Thus, the resulting density and temperature distributions are made consistent.

5. We assume steady-state conditions for an equinox period. During equinox, equatorial symmetry can be assumed, and therefore vector quantities parallel to the magnetic field and first derivatives of scalars

along a field line are zero at the equator. This represents an initial set of boundary conditions.

6. For the second set of boundary conditions, we employ the electron density and temperature measured at some level (Explorer XXII at 1000 km at equinox). In the region in which hydrogen ions are in near chemical equilibrium, the oxygen-hydrogen ion correlation of Equation 8 provides the necessary additional boundary condition required to solve for both ion distributions.

SOLUTION OF EQUATIONS

The continuity equations for the two ion constituents are

$$\frac{\partial}{\partial t}[H^+] = P_H + \frac{9}{8} R[H][O^+] - R[H^+][O] - B\frac{\partial}{\partial s}\left(\frac{[H^+]\, v_{H^+}}{B}\right) = 0 \qquad (9)$$

and

$$\frac{\partial}{\partial t}[O^+] = P_O - \frac{9}{8} R[H][O^+] + R[H^+][O] - B\frac{\partial}{\partial s}\left(\frac{[O^+]\, v_{O^+}}{B}\right) = 0 \qquad (10)$$

where

s = distance on a field line,

t = time,

v = macroscopic transport velocity, parallel to the magnetic field.

B is a function proportional to the intensity of the magnetic field. It is given by

$$B = \frac{1}{r^3} (1 + 3 \sin^2\lambda)^{1/2},$$

where

r = geocentric distance, and

λ = geomagnetic latitude.

This function accounts for the divergence of the magnetic field. The first terms in (9) and (10) express the photoionization rate, the next two terms the charge-exchange process, and the last one the transport process along the magnetic field.

Adding Equations 9 and 10 leads, after integration, to

$$[H^+]\, v_{H^+} + [O^+]\, v_{O^+} = B \int_{s_e}^{s} \frac{(P_O + P_H)}{B}\, ds \equiv C(s) \qquad (11)$$

in which s_e is the field line distance to the equator. In Equation 11 some of the following equatorial boundary conditions are already applied.

$$\left.\begin{aligned} & v_{H^+} = v_{O^+} = f = \lambda = 0 \\ & \frac{\partial N_e}{\partial s} = \frac{\partial [O^+]}{\partial s} = \frac{\partial [H^+]}{\partial s} = \frac{\partial T_e}{\partial s} = 0 \end{aligned}\right\} \; s = s_e. \qquad (12)$$

where

f = acceleration parallel to the magnetic field due to gravitational and centrifugal forces.

The equations of motion for the ions are,

$$\theta_{H^+O^+}\,[H^+]\,[O^+]\,(v_{O^+} - v_{H^+}) + \theta_{O^+n}\,[O^+]\,N_n\,v_{O^+} =$$

$$- kT_e \frac{\partial}{\partial s}\,[O^+] - k[O^+]\,\frac{\partial T_e}{\partial s} + [O^+]m_{O^+}\,f + e[O^+]\,E, \qquad (13)$$

$$\theta_{H^+O^+}\,[H^+]\,[O^+]\,(v_{H^+} - v_{O^+}) + \theta_{H^+n}\,[H^+]\,N_n\,v_{H^+} =$$

$$- kT_e \frac{\partial}{\partial s}\,[H^+] - k[H^+]\,\frac{\partial T_e}{\partial s} + [H^+]m_{H^+}\,f + e[H^+]\,E, \qquad (14)$$

and for the electrons

$$- kT_e \frac{\partial}{\partial s}\,N_e - kN_e \frac{\partial T_e}{\partial s} + N_e m_e\,f - eN_e E = 0, \qquad (15)$$

where

N_n = neutral density,

assuming ambipolar diffusion along field lines and assuming that drag forces between electrons and heavier constituents can be neglected. The coefficient θ_{xy} is related to the diffusion coefficient D_{xy} according to $\theta_{xy} = \dfrac{kT}{([X] + [Y])\,D_{xy}}$. Substituting Equation 15 into Equation 14 and eliminating the electric field and considering $m_e << m_{H^+}$ gives

$$\theta_{H^+O^+}\,[H^+]\,[O^+]\,(v_{H^+} - v_{O^+}) + \theta_{H^+n}\,[H^+]\,N_n\,v_{H^+} =$$

$$- kT_e\,\frac{\partial}{\partial s}\,[H^+] - kT_e\,\frac{[H^+]}{N_e}\,\frac{\partial N_e}{\partial s} - 2k\,[H^+]\,\frac{\partial T_e}{\partial s} + [H^+]m_{H^+}f. \qquad (16)$$

Introducing (11) into (16) results in

$$[H^+]\,v_{H^+} = -\frac{1}{(\theta_{H^+O^+}N_e + \theta_{H^+n}N_n)}\left[kT_e\,\frac{\partial}{\partial s}\,[H^+]\right.$$

$$\left. + k\,\frac{T_e\,[H^+]}{N_e}\,\frac{\partial}{\partial s}\,N_e + [H^+]\left(2k\,\frac{\partial T_e}{\partial s} - m_{H^+}f - \theta_{H^+O^+}C\right)\right] \qquad (17)$$

This leads in connection with continuity Equation 9 and considering conditions 12, to

$$kT_e\,\frac{\partial}{\partial s}\,[H^+] + kT_e\,\frac{[H^+]}{N_e}\,\frac{\partial N_e}{\partial s} + [H^+]\left(2k\,\frac{\partial T_e}{\partial s} - m_{H^+}f - \theta_{O^+H^+}C\right) =$$

$$\left(\theta_{O^+H^+}N_e + \theta_{O^+n}N_n\right)B\int_s^{s_e}\frac{1}{B}\left(P_H + \frac{9}{8}\,R\,[H]\,[O^+] - R\,[H^+]\,[O]\right)ds. \qquad (18)$$

The corresponding relationship for oxygen ions was derived in a similar way, giving

$$k T_e \frac{\partial}{\partial s} [O^+] + k T_e \frac{[O^+]}{N_e} \frac{\partial N_e}{\partial s} + [O^+] \left(2k \frac{\partial T_e}{\partial s} - m_{O^+} f - \theta_{O^+H^+} C \right) =$$

$$\left(\theta_{O^+H^+} N_e + \theta_{O^+_n} N_n \right) B \int_s^{s_e} \frac{1}{B} \left(P_o - \frac{9}{8} R [H] [O^+] + R[H^+] [O] \right) ds. \qquad (19)$$

With the consideration that $N_e = [O^+] + [H^+]$, we have transformed the foregoing relationships into integral equations and solved them numerically by means of an iterative approximation, assuming that the temperature variation is known. The boundary conditions were adopted as described in the previous section.

Assuming that $T_i = T_e$ and adding the energy equations for electrons and ions leads to the energy equation for the electron-ion gas:

$$3k \frac{\partial}{dt} (N_e T_e) = \kappa B \frac{\partial}{\partial s} \left(\frac{T_e^{5/2}}{B} \frac{\partial T_e}{\partial s} \right) + p N_e + q [O]$$

$$- \sum_{x\,y} K_{x+y} [x^+] [y] (T_e - T_n) = 0. \qquad (20)$$

where

κ = Coefficient of the thermal conductivity of the electron gas parallel to the magnetic field.

p = Coefficient for the non-local heating rate,

q = Coefficient for the local heating rate,

K_{x+y} = Coefficient for the local energy loss between ions and neutrals.

The first term represents the heat conduction; the second one expresses the energy gain of the electron gas from fast electrons (nonlocal heating); the third term represents local heating due to photoionization; and the last term represents the local energy loss from ions to neutrals.

We then transformed Equation 20 into an integral equation and solved it numerically by means of an iterative approximation employing the ion composition derived from Equations 18 and 19. The coupling of the energy and continuity equations was accomplished as follows.

First, we assumed that the temperature is constant along the field line and equal to the boundary value given by Explorer XXII. From this, we derived the ion composition by employing Equations 18 and 19. Using these ion distributions, we obtained from Equation 20 a corrected temperature profile which we substituted into Equations 18 and 19, and so on until a suitable precision was obtained. The numerical computation was accomplished on a digital computer.

In the following sections we present the results from a few calculations which provide some quantitative insight into the dependence of the ion composition on variations of energy input and neutral composition and we compare them with experimental results.

RESULTS

To permit comparison of the theory with recent measurements of ion composition, we have calculated the composition and temperature distribution along several field lines. The results for two of these field lines, L = 1.16 and L = 1.84, are described in detail. The shorter field line was chosen because it crosses the equator at the Explorer XXII orbit altitude; therefore we call it the equatorial field line. The longer field line was selected to permit study of the pronounced nighttime electron density enhancement observed by Explorer XXII at some 40° geomagnetic latitude. Thus we call it the midlatitude field line.

As indicated earlier, the boundary conditions used were the electron density and temperature values at 1000 km from Explorer XXII data (1965 vernal equinox, Figures 1 and 2). Furthermore, we adopted the Harris and Priester model 2 ($\bar{F}$ = 75) for the neutral temperature and oxygen concentration. The neutral hydrogen density, a quantity of high uncertainty, was a free parameter to be determined. It will be seen that the concentration of neutral hydrogen sensitively controls the temperature and composition along geomagnetic field lines, therefore we assume a value which is consistent with other satellite measurements. A value of 2×10^5/cc of neutral hydrogen at 500 km was required to provide good agreement between our calculated electron density and Tiros VII measurements at 650 km (Reddy, Brace, and Findlay, 1967). Figure 4 illustrates this agreement which is good, considering the two year difference between Tiros and Explorer XXII measurements. This value is about half of the value of neutral

hydrogen derived in the earlier paper on Explorer XXII results (Brace, Reddy, and Mayr, 1967).

For the energy input, we assumed a fast electron flux of $5 \times 10^7 cm^{-2} sec^{-1}$ consisting of 10 eV electrons having zero pitch angle. This is in the order of the flux given by Hinteregger et al, (1963). Furthermore we assumed the local heating rate at 500 km to be equal to the nonlocal heating rate resulting from the fast electron flux, which is consistent with a result of Geisler and Bowhill, 1965.

The foregoing assumptions concerning the neutral atmosphere and the energy inputs we will hereafter refer to as "realistic". Ion and temperature distributions resulting from the calculations employing these "realistic" assumptions are shown with heavy lines in Figures 5 through 8 for the two field lines, daytime and nighttime. We regard these distributions as representive for solar minimum and shall discuss them further in a later portion of this paper by comparing them with satellite ion measurements

In addition, a parametric study is presented with the aim of providing some quantitative insight into the dependence of our results on the energy input and the neutral atmosphere. The study shows the sensitivity of our results to the inputs and assumptions and thus provides some physical understanding of the effects observed. Table I shows these various assumptions and inputs to the calculations which resulted in distributions labeled a through h in Figures 5 through 8. In the following section we discuss these cases.

Table I

PARAMETRIC STUDY

Case	Condition	Fast Electron Flux ($cm^{-2}sec^{-1}$)	$[H]_{500\ km}$ (cm^{-3})	$[O]_{500\ km}$	Figure
a	Day-Equatorial (realistic)	5×10^7	2×10^5	H & P_{Day}	5
b	Day-Equatorial	0	2×10^5	H & P_{Day}	5
c	Day-Equatorial	5×10^7	4×10^5	H & P_{Day}	5
d	Day-Midlatitude (realistic)	5×10^7	2×10^5	H & P_{Day}	6
e	Day-Midlatitude	0	2×10^5	H & P_{Day}	6
f	Night-Equatorial (realistic)	0	2×10^5	H & P_{Night}	7
g	Night-Midlatitude (realistic)	0	2×10^5	H & P_{Night}	8
h	Night-Midlatitude	0	2×10^5	H & P_{Day}	8

Parametric Study

Figure 5 illustrates three cases (a, b, c) of the daytime equatorial field line.

Case a: Ion concentrations and temperature are plotted versus altitude along the equatorial field line. The heavy lines represent the "realistic" situation described earlier. As this result shows, the ion composition transition level where $[H^+] = [O^+]$ occurs at approximately 830 km. Furthermore the electron temperature decreases along the field line toward the equator. This implies

that the energy loss from ions to neutrals exceeds the heat gain through local and nonlocal heating. It is found in a calculation, whose results are not shown here, that doubling the fast electron flux would lead to a temperature increase along this field line because the resulting energy gain would then exceed the local loss from ions to neutrals.

Case b: To permit quantitative study of the effect of the energy input, both the local and nonlocal heating were assumed to be zero. Thus the heat loss from ions to neutrals is entirely balanced by heat conduction, which produces a significantly stronger temperature decrease than observed with the normal flux in case a. The electron and ion distributions are not significantly changed by the reduction in energy input.

Case c: In order to study the effect of neutral hydrogen, we assumed a concentration of 4×10^5/cc at 500 km, twice the "realistic" value, while the other assumptions remain "realistic". Comparing temperature and density distributions in case a and c reveals the effect of the increase of neutral hydrogen. The temperature decrease is more pronounced than either in case a or b and the N_e gradient is smaller. This change in the temperature profile is due to the increase of the local heat loss to the neutral hydrogen component, which is very effective in cooling protons. Secondly it is due to the change in the ion composition toward an increased relative concentration of protons, which are more efficient than oxygen ions in cooling to neutral hydrogen. This latter enhancement

in the hydrogen ion concentration is produced by the increased neutral hydrogen density through the charge exchange reaction. As a further consequence of increasing neutral hydrogen, the temperature increases at lower altitudes and causes an increase of the oxygen ion scale height in the lower region. Both effects together lead to the appreciable decrease in the electron density at lower altitudes. This example illustrates the sensitivity of the ion composition to the neutral hydrogen density which enabled us to determine the "realistic" value of neutral hydrogen by comparing our results with N_e measurements at 650 km from other satellites.

Figure 6 illustrates two cases (d, e) of the daytime midlatitude field line.

Case d: In this case ion and temperature distributions are shown up to an altitude of 1800 km along the midlatitude field line. As before the heavy lines represent the "realistic" situation. Thus the same assumptions are employed as in case a on the equatorial field line. As seen from this result, the ion transition level occurs at approximately 1000 km for a latitude of some 40° corresponding to this field line. This is a significant change if one considers that this transition occurs at approximately 800 km near the equator (Figure 5), which reflects the relatively strong latitudinal variation of the ion composition.

To study the effect of the latitudinal temperature variation, we calculated the ion distribution along the midlatitude field line using the equatorial electron

temperature from Explorer XXII instead of the actual midlatitude value. This lower temperature causes the transition level on the midlatitude field line to decrease to nearly the same altitude as it was on the equatorial field line. Therefore we can conclude, that the latitudinal variation of ion composition is primarily due to the latitudinal variation of electron temperature, shown in Figure 1.

Examining the altitude variation of the electron temperature in Figure 6 reveals that the temperature increases with altitude along the field line reaching a maximum value of 2700°K at the equator. Comparing this temperature profile with that along the equatorial field line (Figure 5, case a) shows that an inversion of the temperature gradient occurs between these two field lines. One can see an altitudinal temperature decrease along the equatorial field line and a temperature increase along the midlatitude field line. A simple discussion of the energy continuity equation (20) may help to explain this situation. Rewriting Equation 20 in the simplified form

$$\text{const.} \times \frac{\partial^2 T_e^{7/2}}{\partial s^2} = L - G \qquad (20a)$$

shows that the heat conduction term on the left-hand side must balance the difference between the local energy loss, L, and the energy gain, G. Apparently along the equatorial field line, the local loss exceeds the gain, and the conduction term is positive. Therefore, because of symmetry with respect to the equator, T_e exhibits a minimum there and thus must decrease approaching the equator.

On the midlatitude field line, however, the energy gain exceeds the heat loss above 2000 km because the neutral density decreases more rapidly with altitude than does N_e. This situation makes the conduction term in Equation 20a negative at the equator, which intersects the midlatitude field line near 5000 km. Consequently T_e must have a maximum along this field line at the equator and thus the temperature along the midlatitude field line exhibits a positive gradient.

Case e: Analogous to case b in the previous study, case e shows ion and temperature distributions along the midlatitude field line assuming the energy inputs to be zero, but keeping the other conditions "realistic". Again as in case b for the shorter field line the temperature decreases when the flux is removed. The ion composition is only slightly affected by this change in the temperature distribution, a result also evident for the equatorial field line.

Figure 7 shows ion and temperature distributions for the equatorial field line for the "realistic" nighttime conditions.

Case f: The Harris and Priester model was employed, except for the concentration of neutral hydrogen for which we adopted the daytime value, 2×10^5/cc. This reflects the lack of diurnal variation of hydrogen indicated by the model. Heat input was assumed zero.

As expected, the temperature decreases along the field line approaching the equator. A comparison of daytime and nighttime ion distributions (Figure 9)

reveals very strong differences. It appears that the ion transition level decreases approximately 200 km from day to night, decreasing the mean ion mass at 1000 km from 3 amu to nearly 1 amu. This change is caused by both the decrease in T_e and [O] from day to night. It will be shown by means of a study on the mid-latitude field line that the variations of T_e and [O] are of comparable significance in their effect on the ion composition.

Figure 8 illustrates two cases (g, h) of the nighttime midlatitude field line.

Case g: Using "realistic" assumptions described in f, case g shows the ion and temperature distributions along the nighttime midlatitude field line. Again we see that the nighttime temperature decreases with increasing altitude as on the other field line. Similar to the equatorial field line the transition level decreases at night to approximately 600 km from its 1000 km level during the day. Figure 10 permits comparison of the midday and midnight distributions and demonstrates this diurnal change in the transition level.

Case h: In this case the neutral oxygen density at 500 km was increased to its daytime value to observe the effect on the transition level. This placed the transition level at 750 km rather than at 600 km as in the "realistic" nighttime case, g. From this we conclude, that the diurnal variation of both the electron temperature and the neutral atmosphere significantly influence the ion composition.

Figure 11 permits comparison of the "realistic" daytime and nighttime ion distributions at midlatitude. The electron density increases all along this midlatitude field line from day to night. Consistent with satellite measurements (Reddy, Brace, and Findlay, 1967) the electron density at 600 km shows little variation from daytime to nighttime at this latitude. Since the decrease of the electron temperature and neutral oxygen concentration lowers the transition level to approximately 600 km at night, the associated electron density scale height increases and leads to the observed midlatitude enhancement of N_e at 1000 km, shown in Figure 2.

This parametric study has allowed us to describe some features of the topside ionosphere and to evaluate their dependence on the energy inputs and the neutral atmosphere. On this basis, we shall now discuss the results more generally and compare them with satellite ion composition measurements.

Discussion and Comparison with Other Results

Some of the most striking features of our results can best be described as follows:

1. In the daytime there is a negative temperature gradient along low latitude field lines and a positive temperature gradient along midlatitude field lines.

2. In the daytime the ion transition level exhibits a latitudinal variation from 800 km near the equator to 1000 km at midlatitudes.

3. The altitude of the transition level decreases at night to about 600 km both at the equator and at midlatitudes.

4. The electron content in the midlatitude protonospheric field tube is greater at night than during day.

The foregoing study leads to the following interpretation of the above major features.

1. Because of the spatial variation of heat gain and loss of electrons and ions along field lines, the balancing heat conduction can lead to an altitudinal temperature decrease along equatorial field lines and for the same conditions can lead to a temperature increase along midlatitude and high latitude field lines. One could describe this feature by stating that, in the topside ionosphere, the temperature gradient increases with increasing latitudes. We have shown in Figure 12 the latitudinal behavior of the electron temperature deduced from our calculations along several field lines under daytime conditions. Successive temperature values on each field line are connected by thin lines thus showing the altitudinal temperature gradient along individual field lines. As a consequence of this latitudinal temperature gradient the temperature

minimum at the equator becomes more pronounced with increasing altitude. It also appears that the temperature maximum at midlatitudes moves poleward at higher altitudes.

2. Primarily as a consequence of the daytime latitudinal temperature variation the ion composition varies with latitude. The calculated ion composition is shown in Figure 13, where the mean ion mass versus latitude is plotted for various altitudes. Figure 14 shows a comparison of these daytime results with the mean ion mass at 800 km derived from Alouette I data by Thomas et al. 1966. The agreement is good. Ion spectrometer measurements from OGO-C (Taylor, private communication, 1966) also agree with our calculated results.

3. Primarily as a consequence of the diurnal variation of the electron temperature and neutral oxygen concentration, the ion transition level decreases at night as shown in Figure 11, where these levels are plotted versus latitude. The nighttime ion composition from which the transition levels in Figure 10 are derived is shown in Figure 15 as latitudinal variation of the mean ion mass at various altitudes. Figure 14 also shows a comparison with Alouette nighttime values of mean ion mass. The agreement is quite acceptable.

4. The enhancement of the electron density from daytime to nighttime along the midlatitude field line, shown in Figure 10, occurs because the

decrease of the T_e and [O] from day to night lowers the ion composition transition level and consequently increases the density scale height at lower altitudes.

Figure 10 clearly reveals that a charged particle conservation in the protonospheric field tube does not exist because of the electron density enhancement at all altitudes above 500 km along the midlatitude field line. It appears that this behaviour is not necessarily in contradiction to the diffusion barrier described by Hanson and Ortenburger (1961). The nighttime enhancement in the midlatitude protonosphere may instead result from the very fast decrease of neutral oxygen and the less pronounced decrease of oxygen ions above this diffusion barrier because of the charge exchange reaction there. While neutral oxygen diffuses downwards at night, more oxygen ions transfer their charge to hydrogen atoms than do protons to neutral oxygen; thus the proton concentration increases. The loss to the oxygen ion population through conversion to protons via charge-exchange could be continuously replaced by an upward diffusion of oxygen ions. In this case, the diffusion barrier represented by the protons is less effective than in the case where protons must diffuse through oxygen ions into the protonosphere. Whether this mechanism is actually responsible for the described diurnal variation in the protonosphere is an open question demanding a study of the dynamic protonosphere-ionosphere coupling.

A few points regarding the limitations in this investigation need to be noted. The region investigated was limited to the topside ionosphere above about 500 km. Therefore it was necessary to make calculations based on empirical boundary conditions for electron density and temperature, which in a sense represent the entire region below that considered here. Therefore our results depend upon boundary conditions not theoretically described or explained in this paper. Consequently this paper does not attempt to completely explain the behaviour of T_e and N_e in the topside ionosphere. For the relative ion composition, however, this limitation does not exist. We derived the relative ion concentration of H^+ and O^+ without a priori assumptions concerning it. This was possible because the composition is controlled by charge exchange rather than transport processes at the lower boundary of the region where we started the calculation. Thus the description of the ion composition and its temperature dependence can be regarded as independent of processes controlling the lower F-region, and therefore some understanding of the compositional behavior of the topisde ionosphere has been gained.

High Latitudes

A second limitation of this investigation was the restriction to low and mid-latitudes. Above 50° our calculations failed to describe properly the ion composition in the topside ionosphere. The observed latitudinal variation of the mean ion mass at 800 km (Thomas et al., 1966) shows a rapid increase above 50°, already

reaching 16 amu at 60°. This is in contrast to our result shown in Figure 14 from which it appears that the mean ion mass decreases toward higher latitudes after passing a maximum value at some 45°.

Another observed feature of the topside ionosphere is the very rapid decrease of ion concentration observed from the OGO-A satellite (Taylor et al., 1965), when traversing high latitude field lines at high altitudes. Regarding these two observations as characteristic for high latitudes, it is possible to relate them, and to explain why our approach does not predict them.

Let us assume that there exists an upward flux of protons into the protonosphere, in contrast to the concept employed in this study. The effect of such a flux is to decrease the proton concentration above the charge exchange region and thus to increase the $O^+ - H^+$ transition level. Consequently an increase of this flux with latitude could properly account for the above described observations and their deviation from our result at high latitudes.

So the question arises as to how such an upward flux and its latitudinal increase can be understood. For steady state conditions the concept of diffusion along field lines (applied in this paper) implies that such a flux cannot arise because of the lack of chemical sinks in the protonosphere. So we postulate, that diffusion across field lines may be of importance in the sense that this diffusion flux integrated over the protonospheric field tube must be balanced by a proton flux through the bottom of the tube into the protonosphere. This integrated

diffusion flux depends firstly upon the density gradient across the magnetic field tube and secondly upon the volume of the tube. At higher latitudes, where the field tubes become very large, the plasma diffusion across the field becomes more significant and thus may cause the desired enhancement of the upward flux at high latitudes. This in turn decreases the proton concentration and affects the density gradient across field lines. Thus through diffusion across field lines a strong coupling may exist at high latitudes between the density on a field line and the density gradient across the field line. So actually this coupling may effectively contribute to the observed high latitude features of the topside ionosphere.

In order to maintain these fluxes and gradients across field lines ionization has to be removed. This is possible through an escape of protons in the polar region, where the field line configuration permits it. Such an escape of protons could lead to an appreciable reduction in the proton concentration at the poles and thus could maintain the density gradient across high latitude field lines in the protonosphere, which may effectively reduce the concentration even at midlatitudes through diffusion across field lines. It will be our future task to study this etfect quantitatively.

SUMMARY

The particle and energy continuity equations for electrons, protons, and oxygen ions were simultaneously solved. By considering the primary source of protons to be resonance charge-exchange between oxygen and hydrogen ions, the spatial distribution of the two ion species could be derived without any assumption concerning their relative concentration. The electron density from Explorer XXII at 1000 km was adopted as the boundary condition for the ion composition. Temperature data from Explorer XXII measurements were employed as boundary values to derive the temperature profiles. Because of dependence of temperature and density distributions on the energy inputs and the neutral gas composition, a study was conducted to obtain a quantitative insight into various effects. The ion distribution is very sensitive to the neutral hydrogen concentration. Therefore, by comparing our results with electron densities from Tiros VII we deduced a neutral hydrogen density of some $2 \times 10^5/cm^3$ at 500 km. Based on this value, we could show that the equatorial temperature minimum during day time (Figure 1) is associated with a temperature decrease along the corresponding field line, whereas the temperature maximum at some 40° latitude corresponds to a temperature increase up to high altitudes. Thus the latitudinal temperature variations is a feature of this change of temperature gradient, which is a natural consequence of the energy balance along different field lines.

The ion distribution derived for the daytime shows a strong latitudinal variation, so that the ion composition transition level increases from 800 km at the equator to 1000 km at 40° latitude. This variation is in very good agreement with ion spectrometer measurements and the latitudinal variations of the mean ion mass derived from Alouette I. An investigation revealed that this variation of the ion composition is primarily caused by the latitudinal variation of the electron temperature, of which we claim to have some understanding. Studying the nighttime situation, we could show that the ion composition transition level occurs at about 600 km. Both the nighttime decrease of the plasma temperature and the change in the neutral composition were found to be of comparable importance for this decrease of the transition level. Our nighttime results also agree well with ion compcsition data derived from Alouette. Furthermore, it was shown that the observed nighttime enhancement of N_e near 40° latitude is strongly influenced by the nighttime decrease of electron temperature and neutral oxygen. It appears that this enhancement occurs not only at 1000 km, as indicated by Explorer XXII (Figure 2), but all along the corresponding field line up to the equator. Thus the concept of conservation of ionization cannot be valid in this midlatitude field tube since a diurnal exchange of ionization between the ionosphere and protonosphere occurs.

Acknowledgment

This work was performed while one of us (H. G. Mayr) was a NAS-NRC post-doctoral resident research associate.

REFERENCES

1. Bauer, S. J., The Constitution of the Topside Ionosphere, Presented at the NATO Advanced Study Institute, Norway, 1965.

2. Brace, L. H., N. W. Spencer, and A. Dalgarno, Detailed Behavior of the Midlatitude Ionosphere from Explorer XVII Satellite, Planet. Space Sci., 13, 647-666, 1965.

3. Brace, L. H., B. M. Reddy, Early Electrostatic Probe Results from Explorer XXII, J. Geophys. Res., 7', 5783-5792, 1965.

4. Brace, L. H., B. M. Reddy and H. G. Mayr, Global Behavior of the Ionosphere at 1000 km Altitude, NASA-Report X-627-66-362, 1966. To be published in J. Geophys. Res., 1967.

5. Dalgarno, A., B. M. McElroy, and R. J. Moffett, Electron Temperatures in the Ionosphere, Planet. Space Sci., 11, 463-484, 1963.

6. Geisler, J. E., and S. A. Bowhill, An Investigation of Ionosphere-Protonosphere Coupling, Aeronomy Report No. 5, University of Illinois, Urbana, 1965.

7. Hanson, W. B., and I. B. Ortenburger, The Coupling Between the Protonosphere and the Normal F-Region, J. Geophys. Res., 66, 1425-1435, 1967.

8. Harris, I., and W. Priester, The Upper Atmosphere in the Range From 120-800 km, Brought Out by the Institute for Space Studies, GSFC-NASA, 1964.

9. Hinteregger, H. E., L. A. Hall and G. Schmidtke, Solar XUV Radiation and Neutral Particle Distribution in July 1963 Thermosphere, Presented at the Fifth Inst. Space Science Symposium, Florence, May 1964, Space Res. V, Edited by D. G. King-Mele, North Holland Publishing Company, 1965.

10. Johnson, F. S., The Ion Distribution Above the F_2-Maximum, J. Geophys. Res., 65, 577-584, 1960.

11. Reddy, B. M., L. H. Brace and J. A. Findlay, The Ionosphere at 640 km on Quiet and Distrubed Days, NASA-Report, 1966.

12. Spitzer, Jr., L., Physics of Fully Ionized Gases, Interscience Tracts on Physics and Astronomy, 1965.

13. Taylor, Jr., H. A., A. C. Brinton, and L. R. Muenz, First Results from OGO-C Ion Composition Experiment, Presented at the 47th Annual Meeting of the AGU, March 1966.

14. Taylor, Jr., H. A., H. C. Brinton, and C. R. Smith, Positive Ion Composition in the Magnetosphere Obtained From the OGO-A Satellite, J., Geophys. Res., 70, 5769-5781, 1965.

15. Thomas, F. O., M. H. Rycroff, C. Colin and K. L. Chan, Electron Density Profiles in Ionosphere and Exosphere, Proceeding of the NATO Advanced Study Institute held at Finse, Norway, Edited by Jon Fihapen, North Hollywood Publishing Co., Amsterdam, 1966.

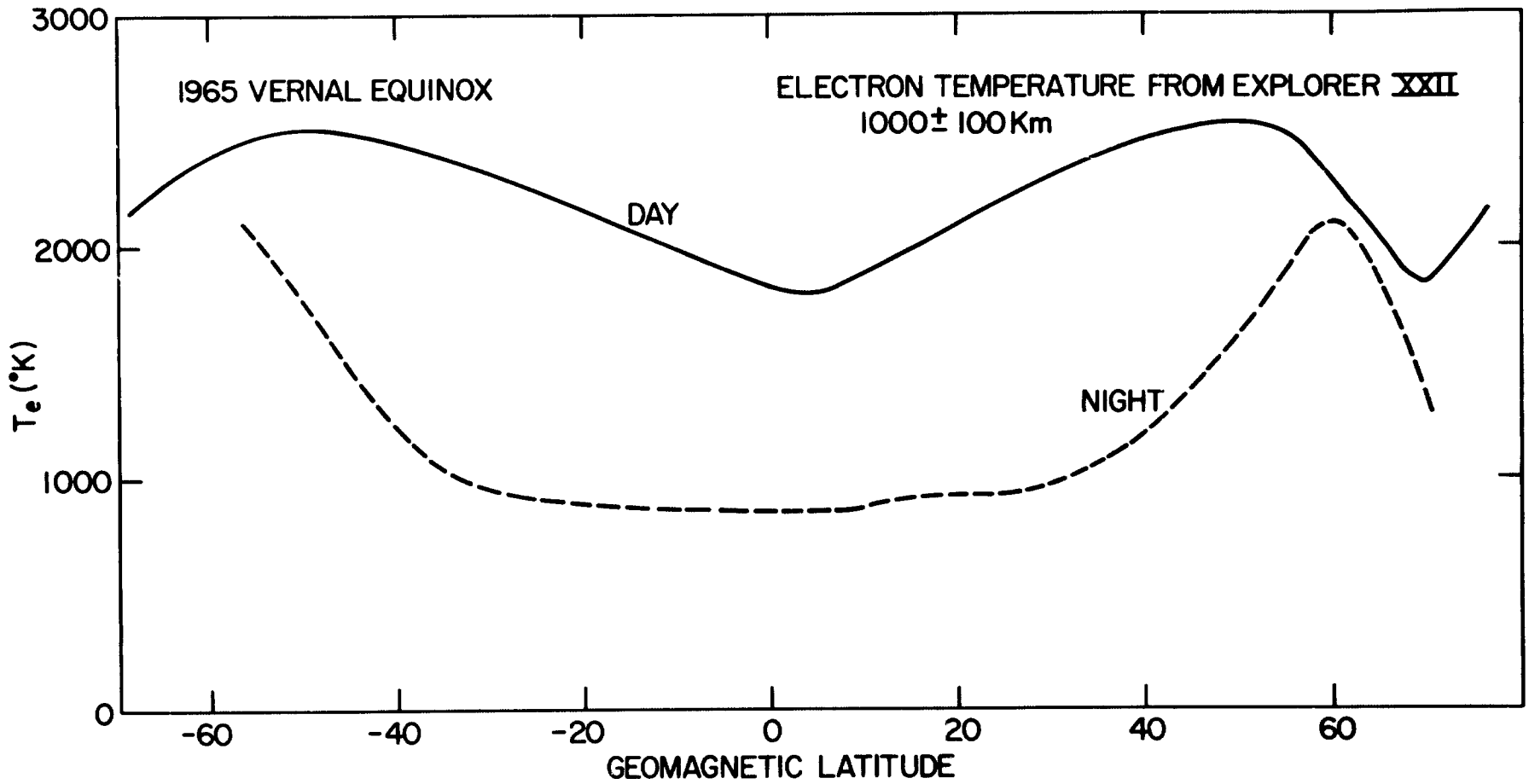

Figure 1. Explorer XXII measurements of T_e employed as boundary conditions for the calculations.

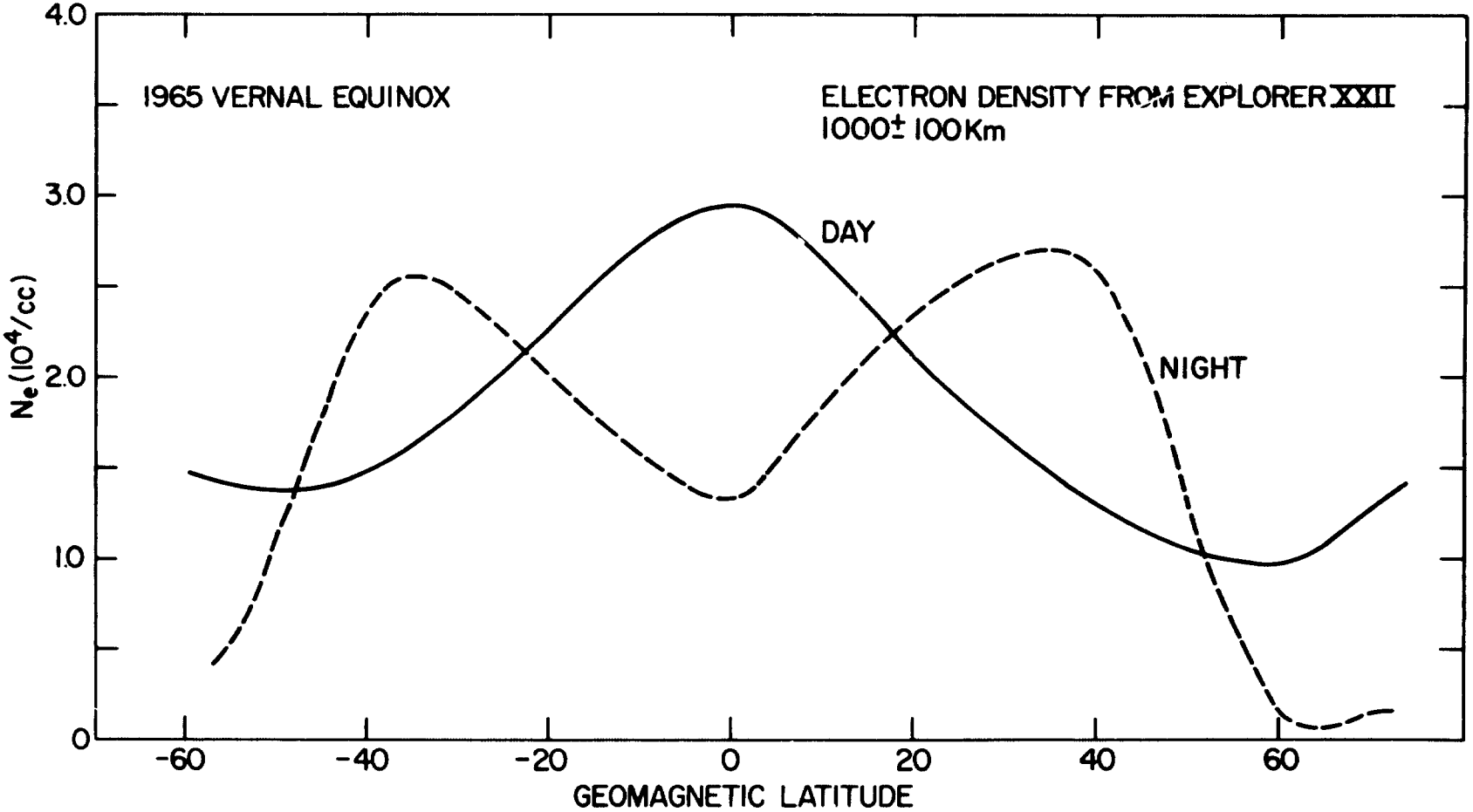

Figure 2. Explorer XXII measurements of N_e employed in the calculations.

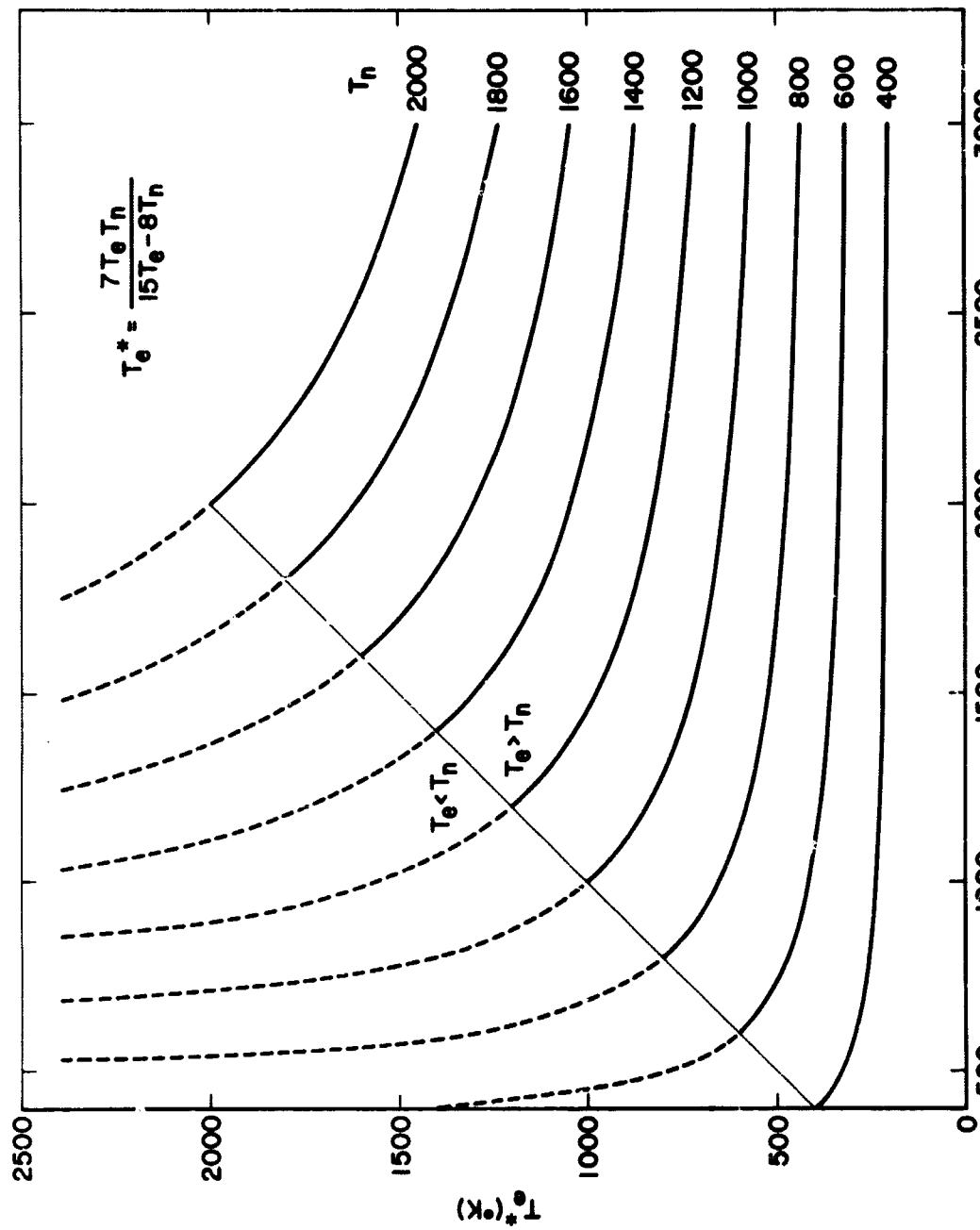

Figure 3. Reduced temperature T_e^*.

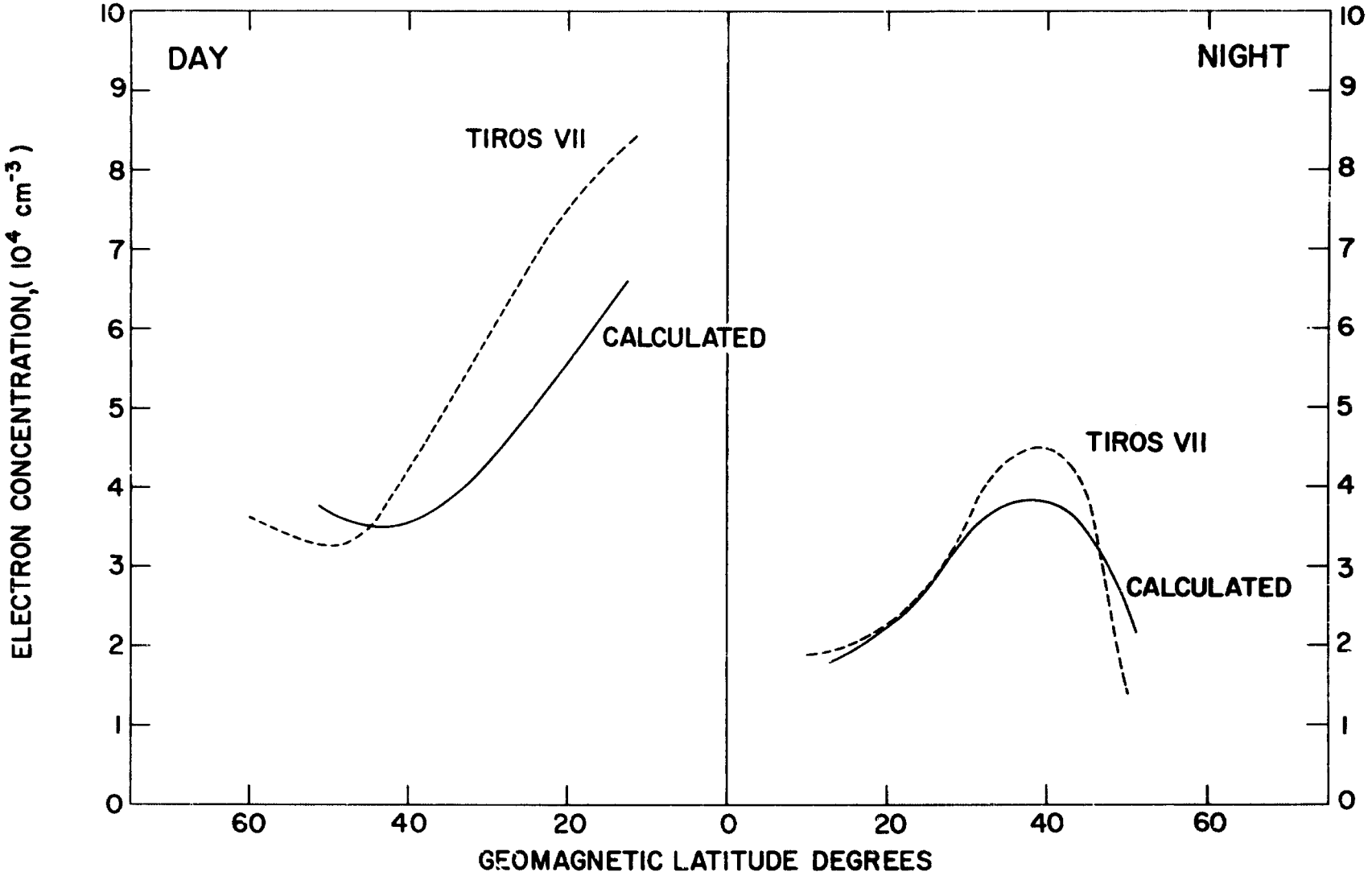

Figure 4. Comparison of calculated N_e with TIROS VII measurements were at 650 km, assuming $[H] = 2 \times 10^5 cm^{-3}$. Since the TIROS VII measurements were not taken at equinox, they were normalized by averaging northern and southern hemisphere data.

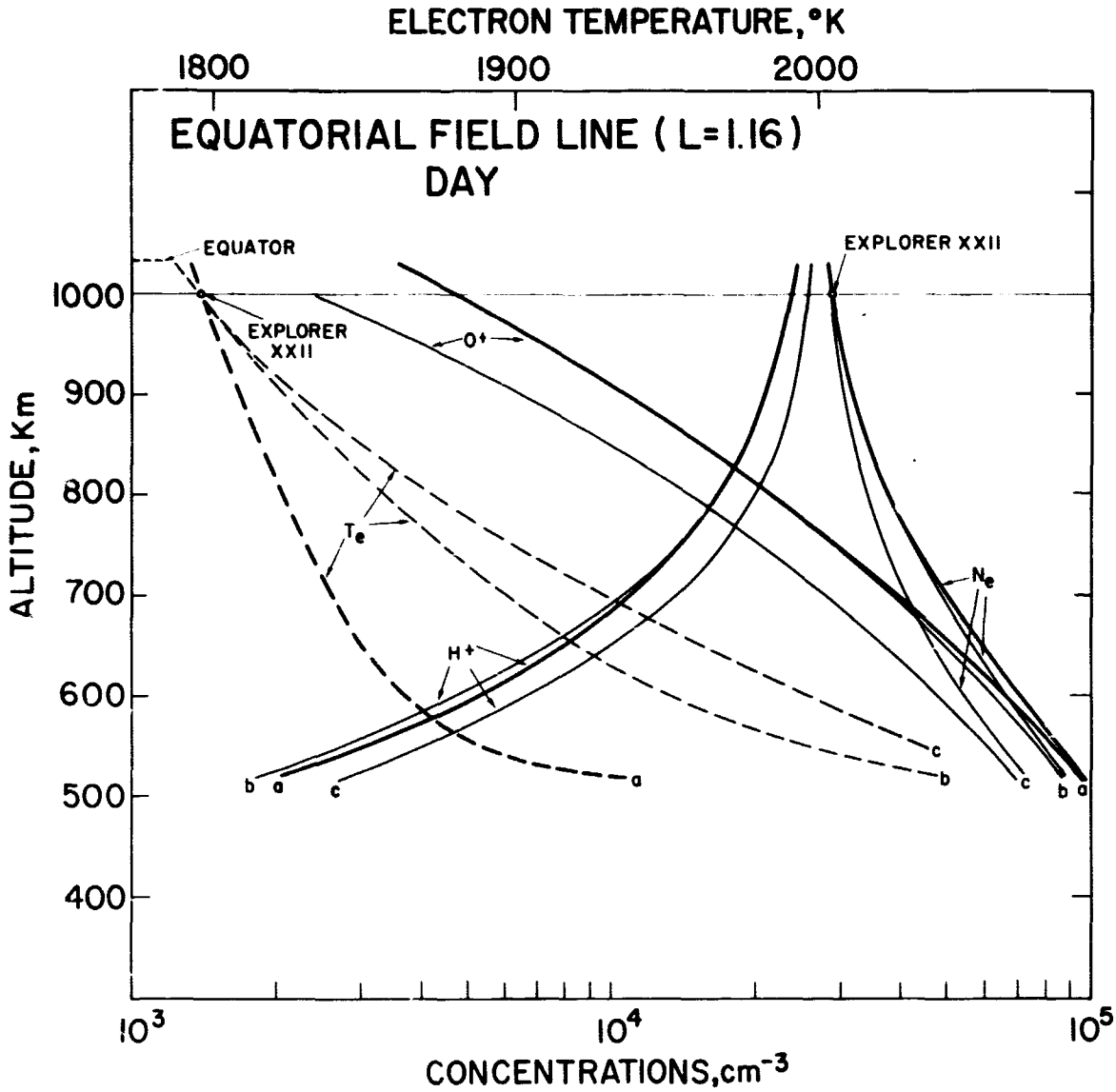

Figure 5. Calculated T_e and composition profiles along the daytime equatorial field line for case a (realistic), case b (zero heating) and case c (high neutral hydrogen). See Table I for detailed assumptions. Explorer XXII inputs of T_e and N_e at 1000 km are shown.

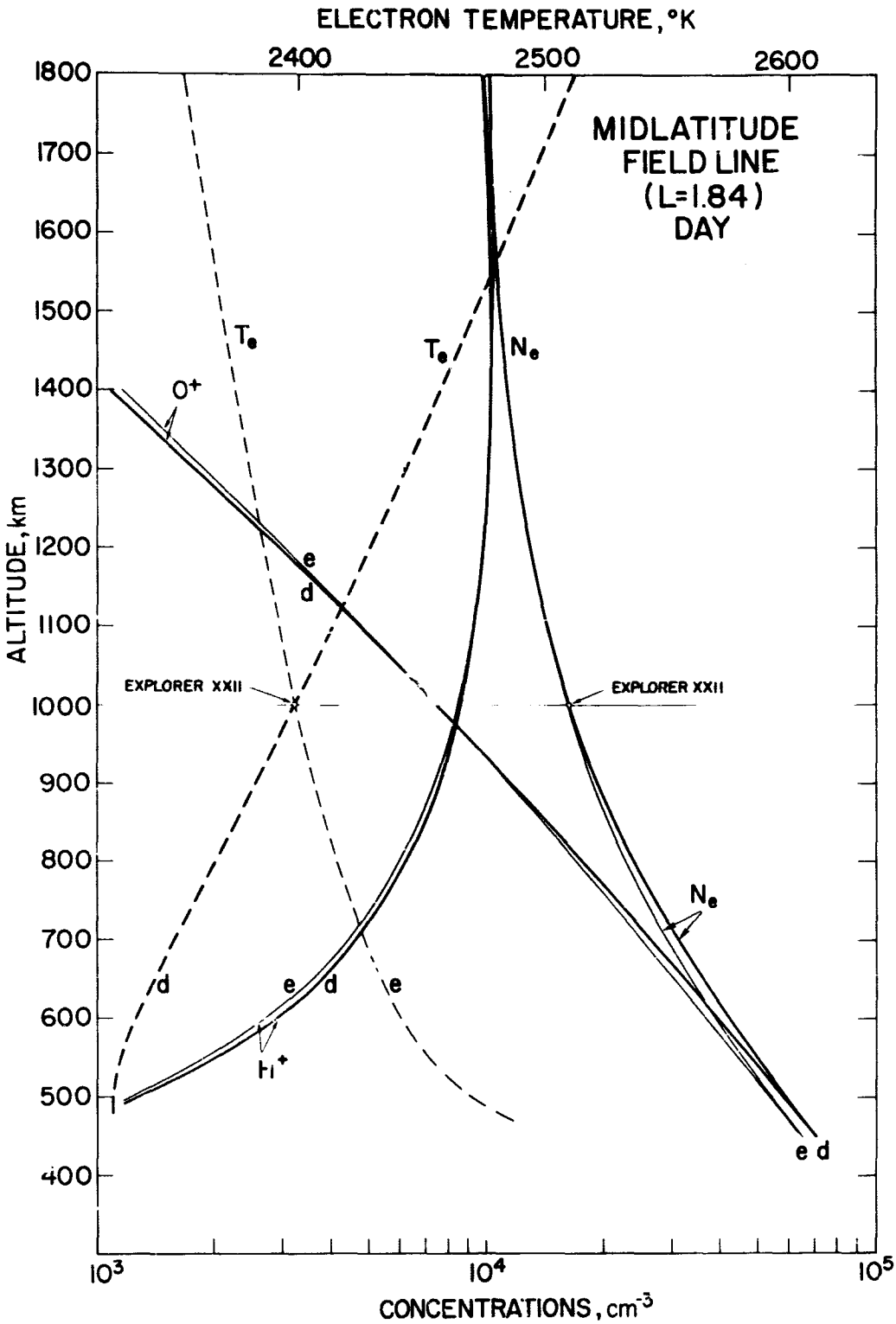

Figure 6. Calculated T_e and composition profiles along the daytime midlatitude field line for case d (realistic) and case e (zero heating). See Table I for further details.

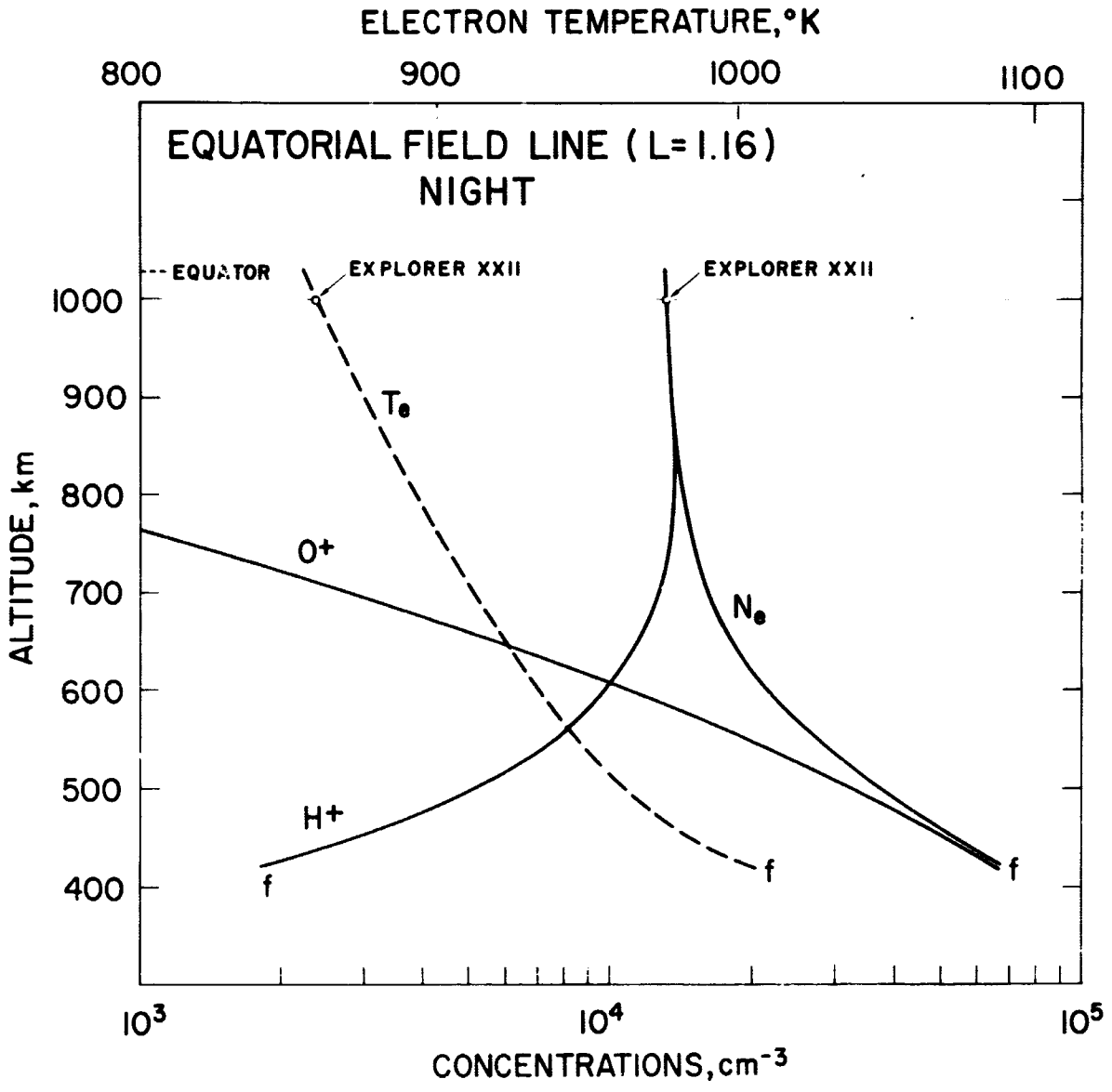

Figure 7. Calculated T_e and composition profiles along the nighttime equatorial field line for the "realistic" case f, shown in Table I.

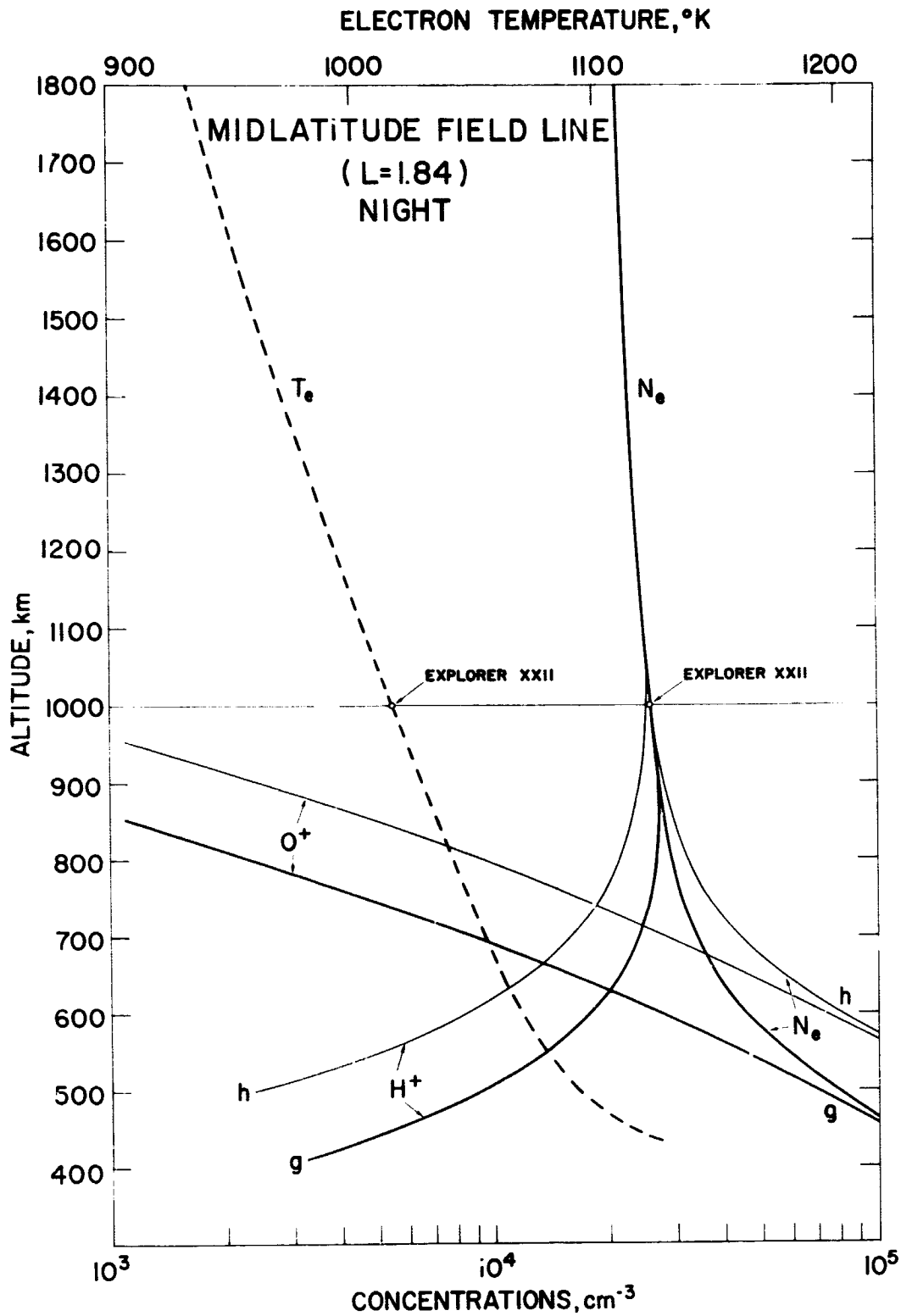

Figure 8. Calculated T_e and composition profiles along the nighttime midlatitude field line for case g (realistic) and case h (high atomic oxygen).

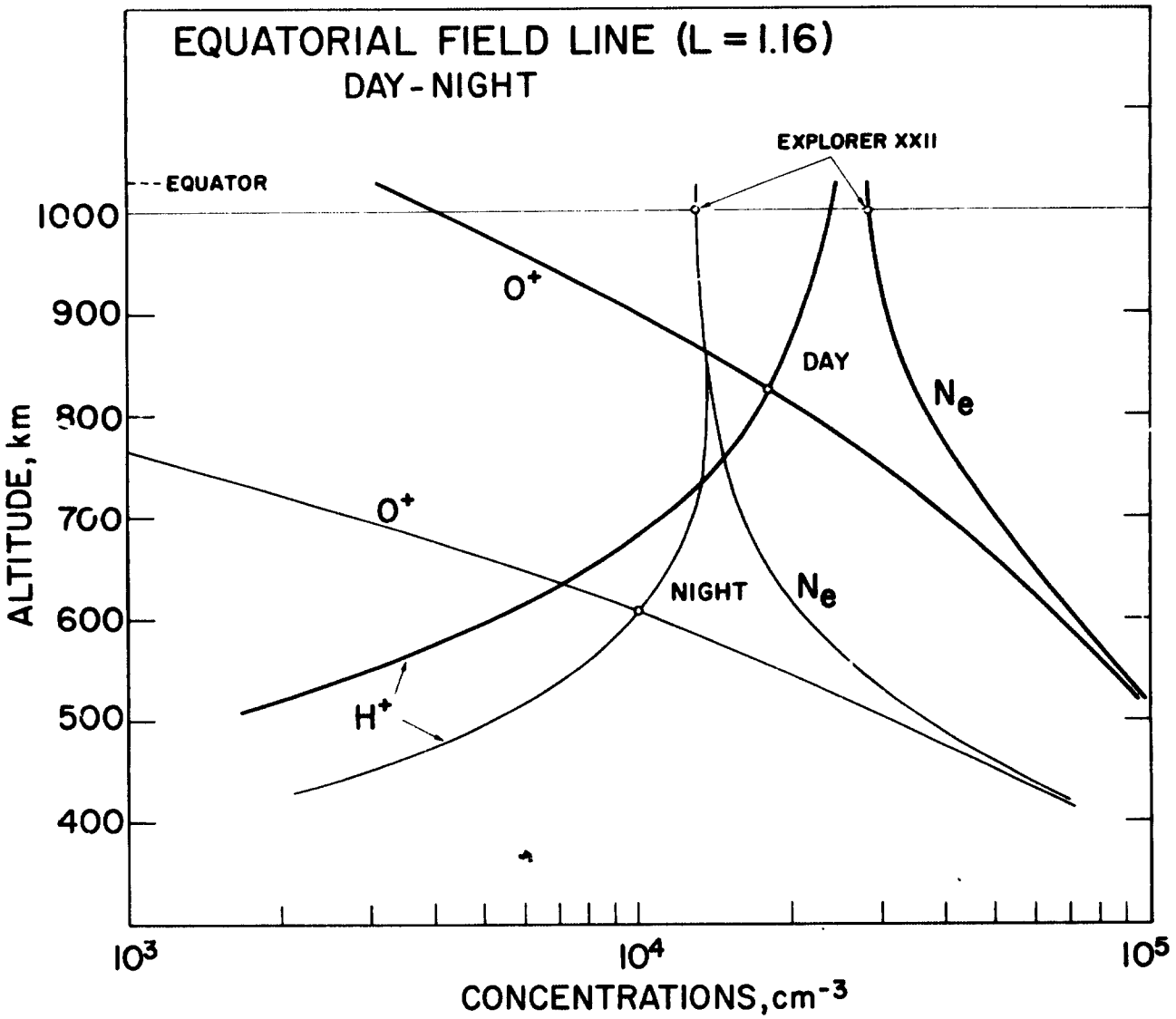

Figure 9. Comparison of day and night ion composition profiles along the equatorial field line. Note the decrease of the $O^+ - H^+$ transition level from 830 km in the daytime to 600 km at night.

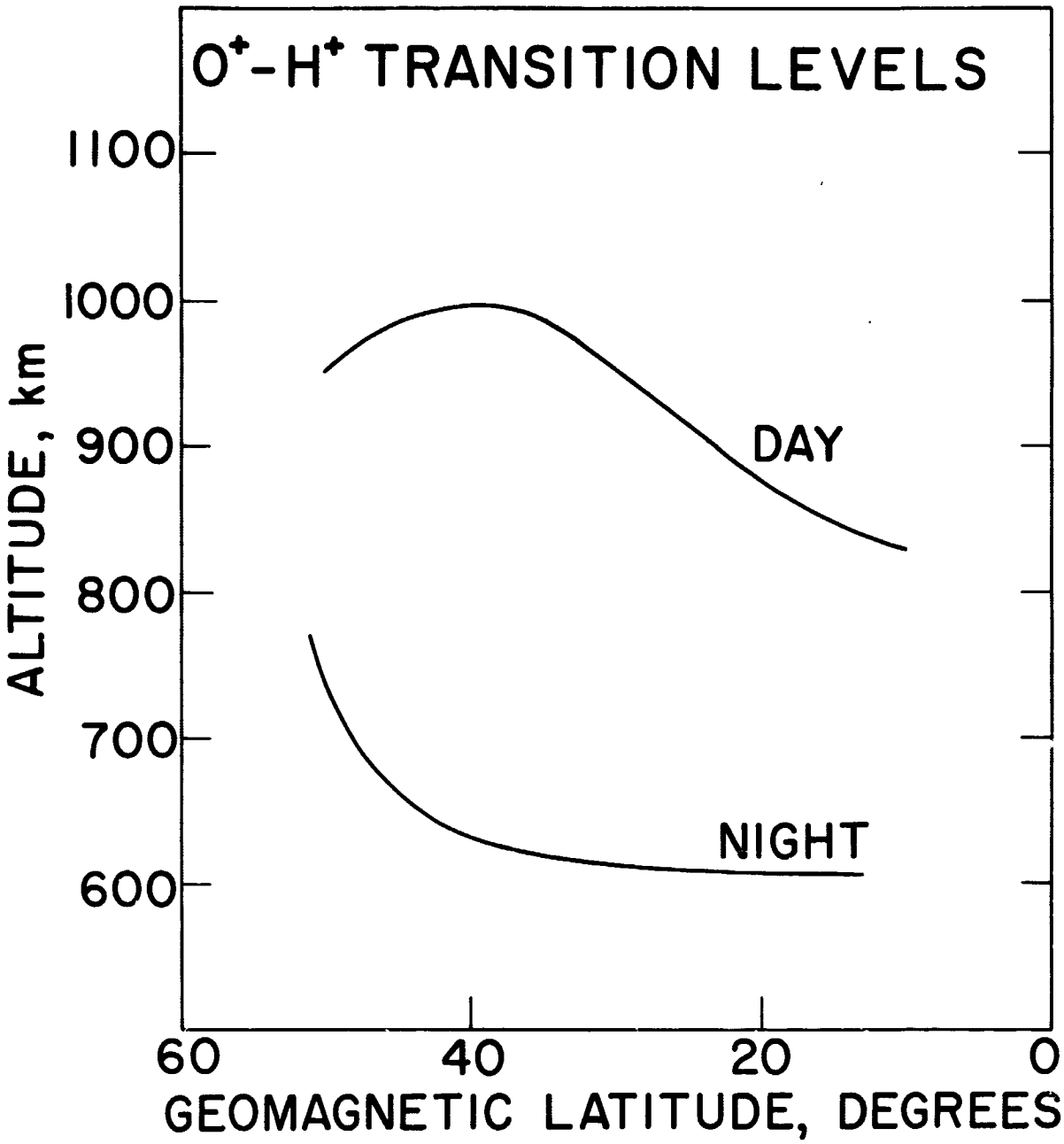

Figure 10. Calculated latitudinal variation of the transition level for midday and midnight.

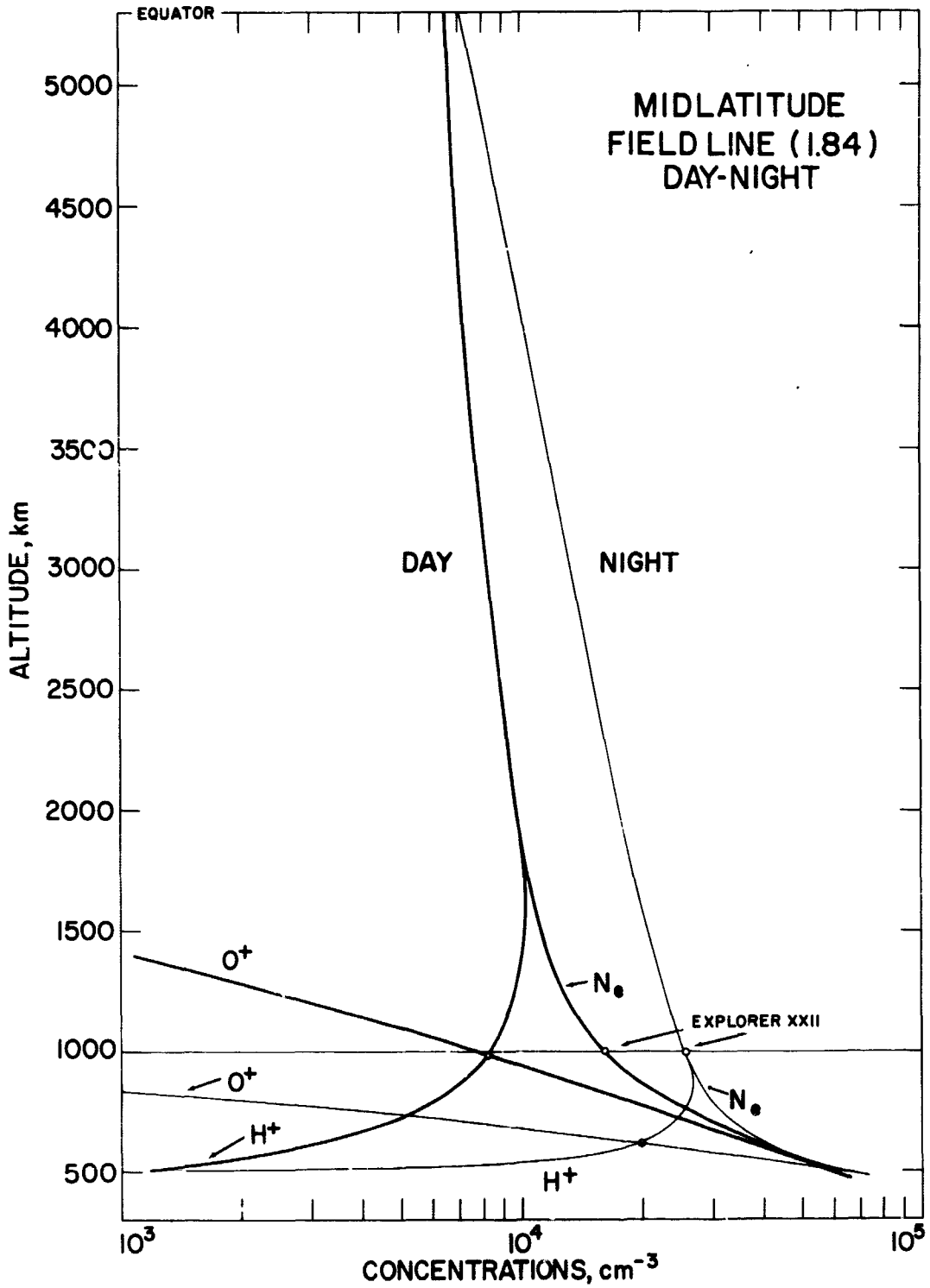

Figure 11. Comparison of day and night ion composition profiles along the midlatitude field line. Note the nighttime enhancement along the entire field line above 500 km.

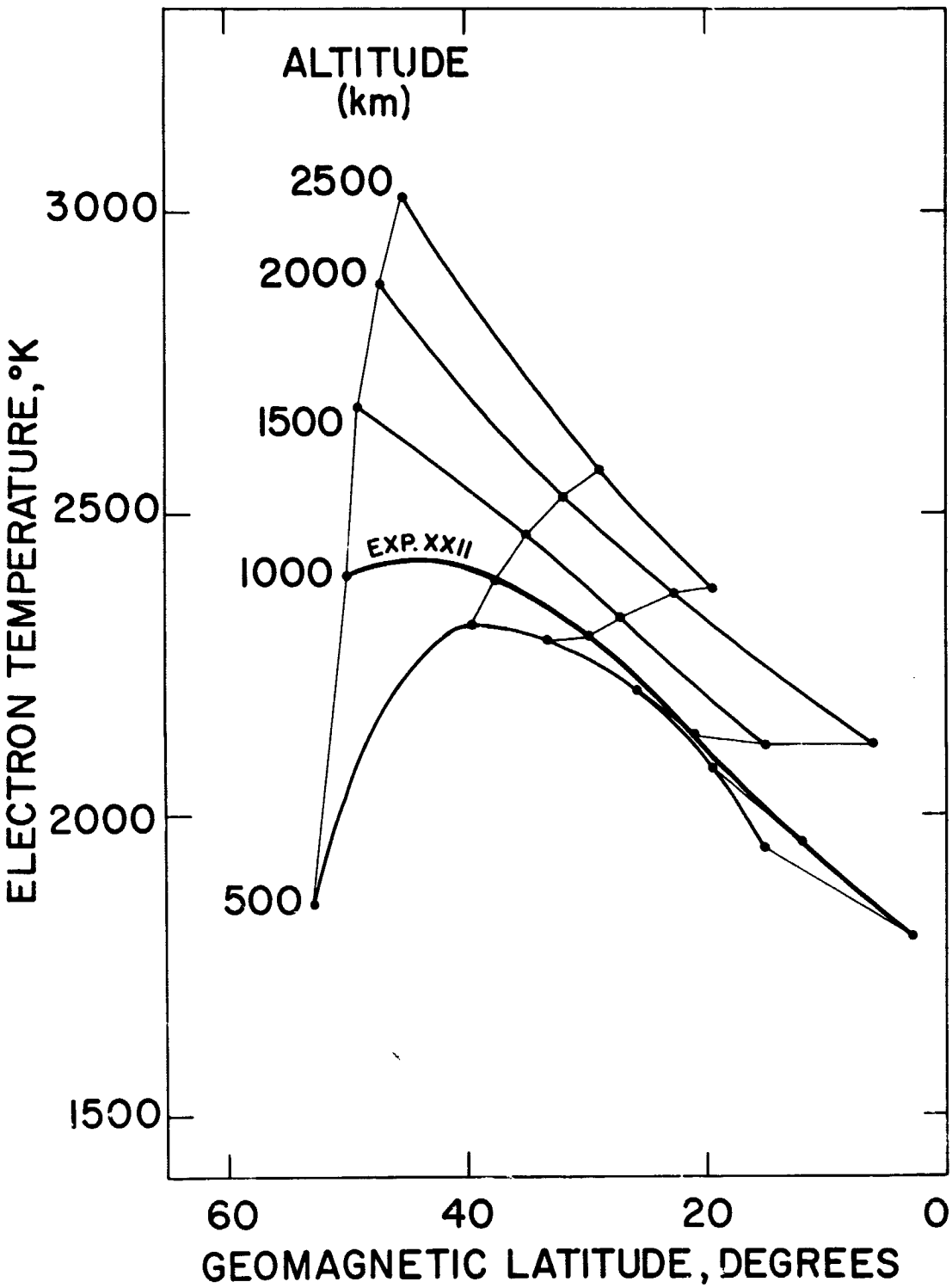

Figure 12. Calculated latitudinal variation of T_e at various altitudes. The Explorer XXII measments employed in the calculation are shown with heavy line (1000 km). The points represent the values calculated at the indicated altitudes along various field lines and are connected by thin lines.

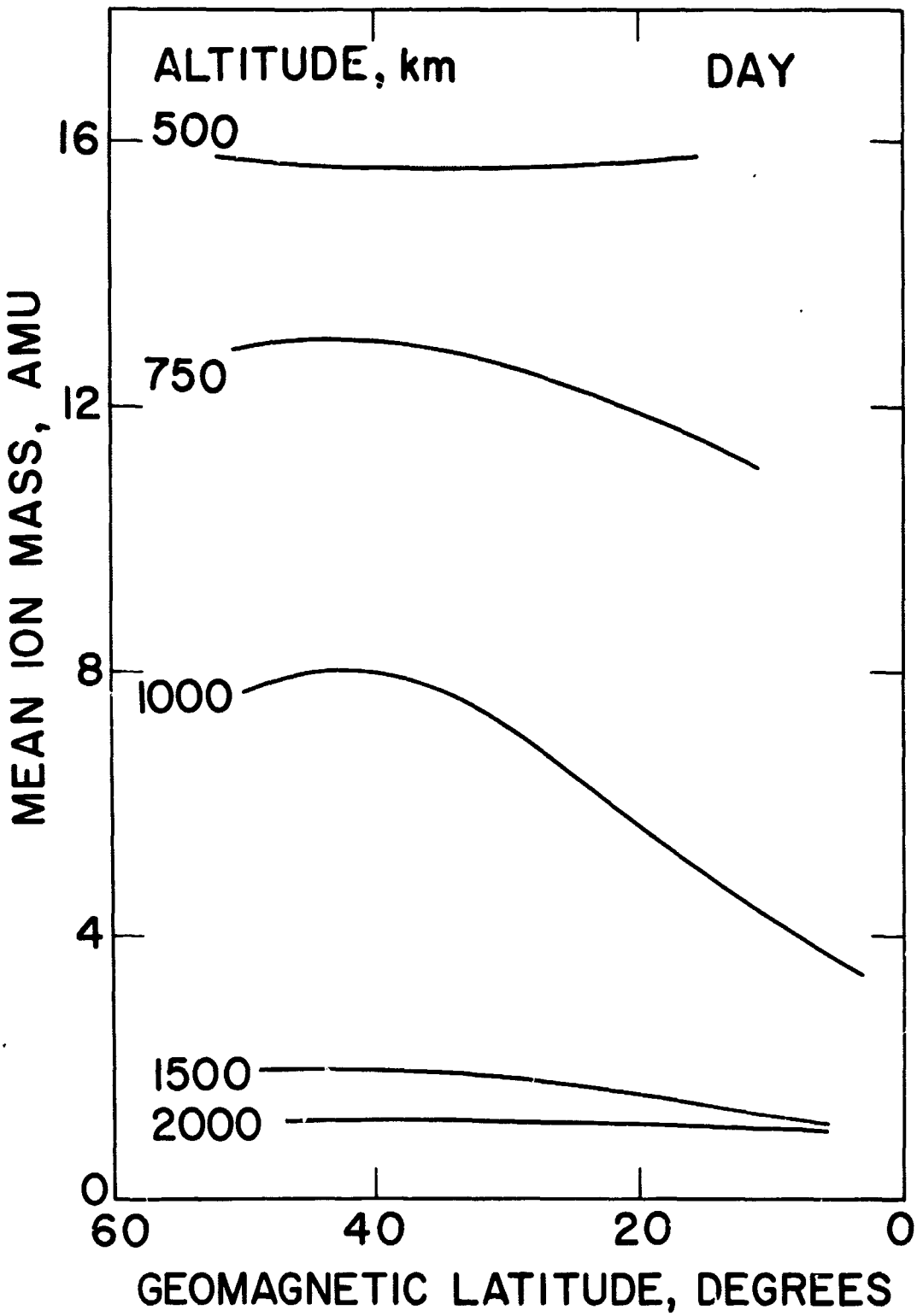

Figure 13. Calculated daytime mean ion mass variation with latitude at various altitudes.

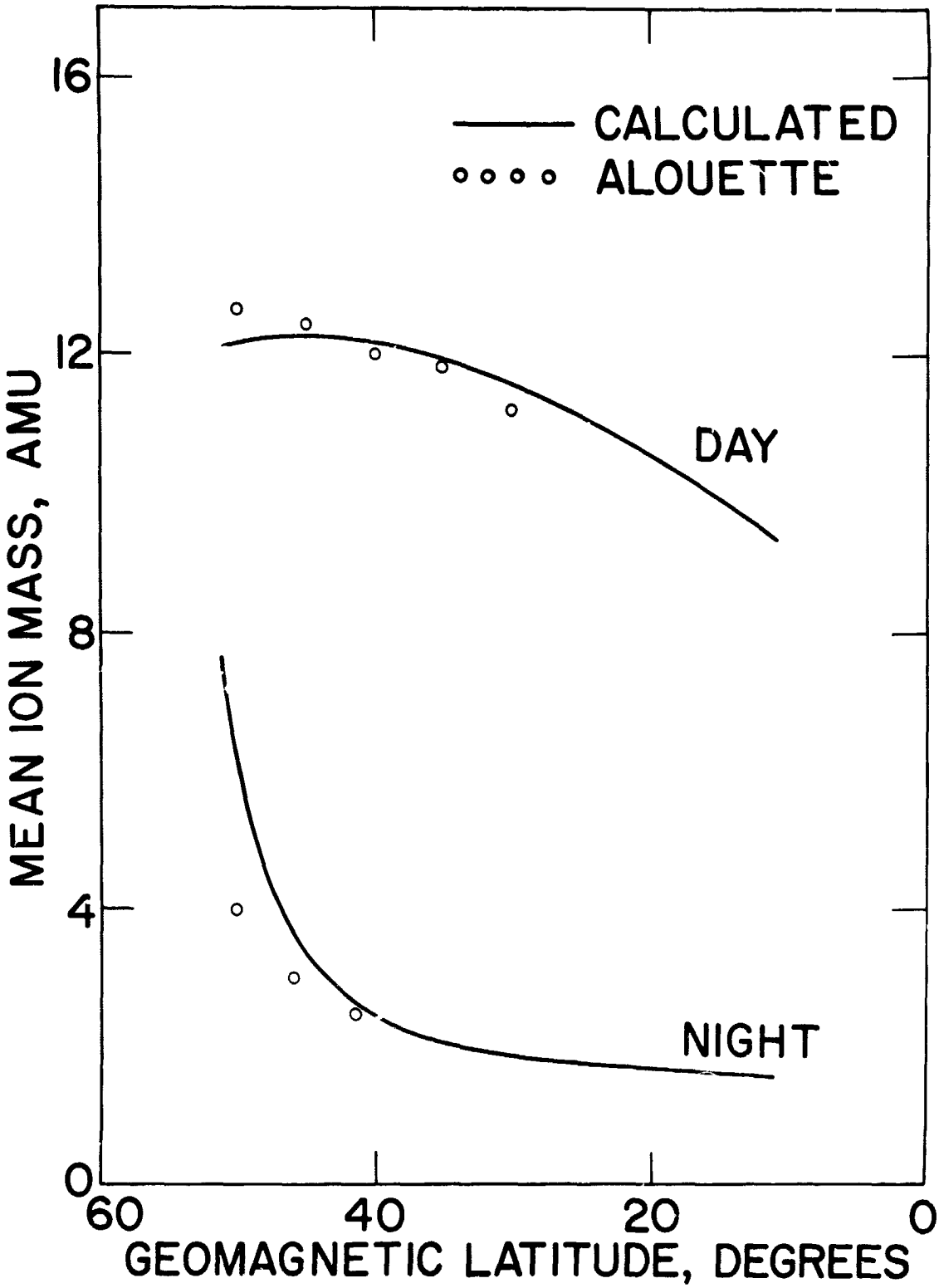

Figure 14. Comparison of calculated mean ion mass at 800 km with those derived from Alouette I topside sounder measurements for the same altitude (Thomas, et al.).

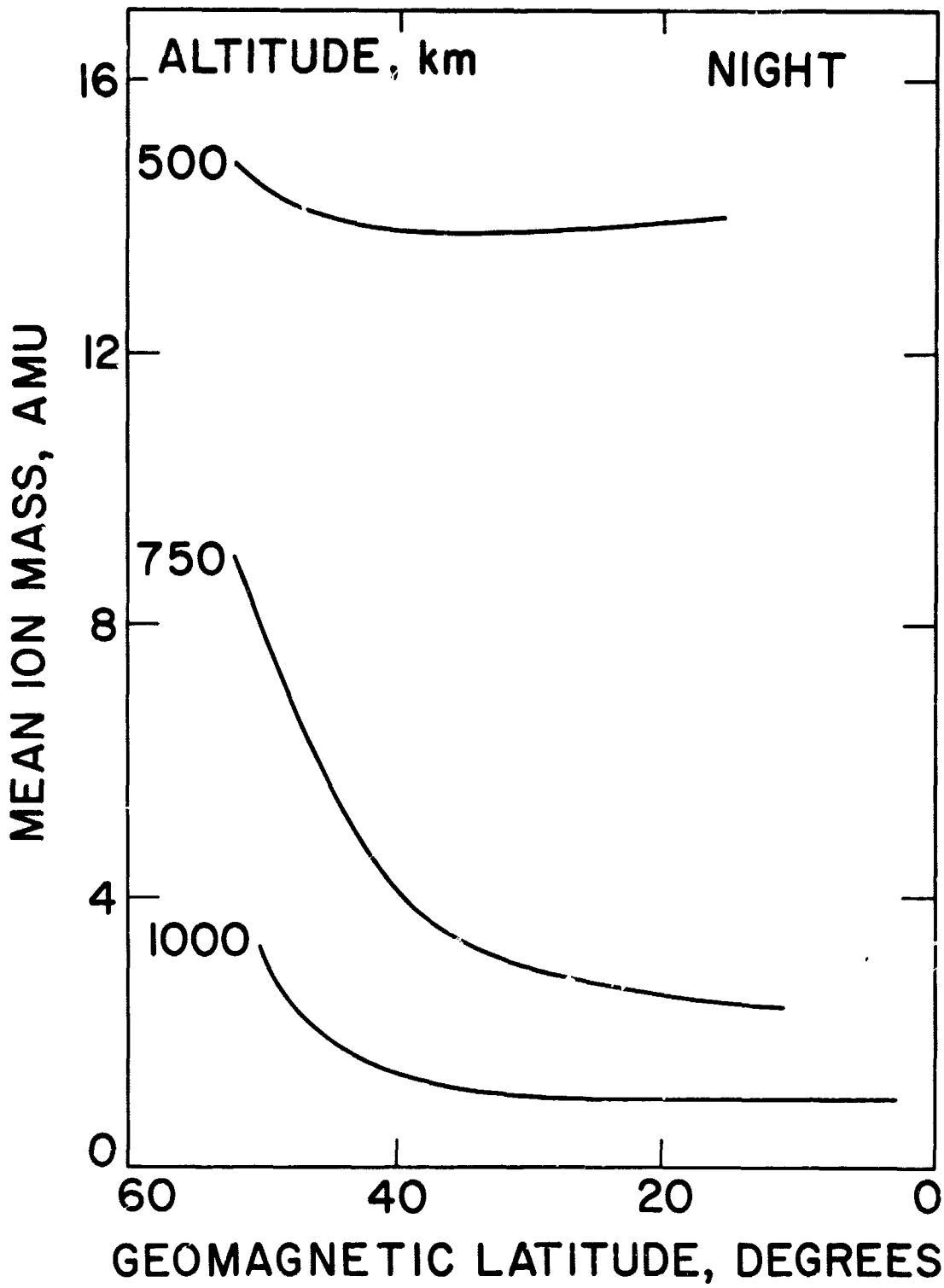

Figure 15. Calculated nighttime mean ion mass variation with latitude at various altitudes.